avantium

High-Throughput Systems for Fischer-Tropsch Applications

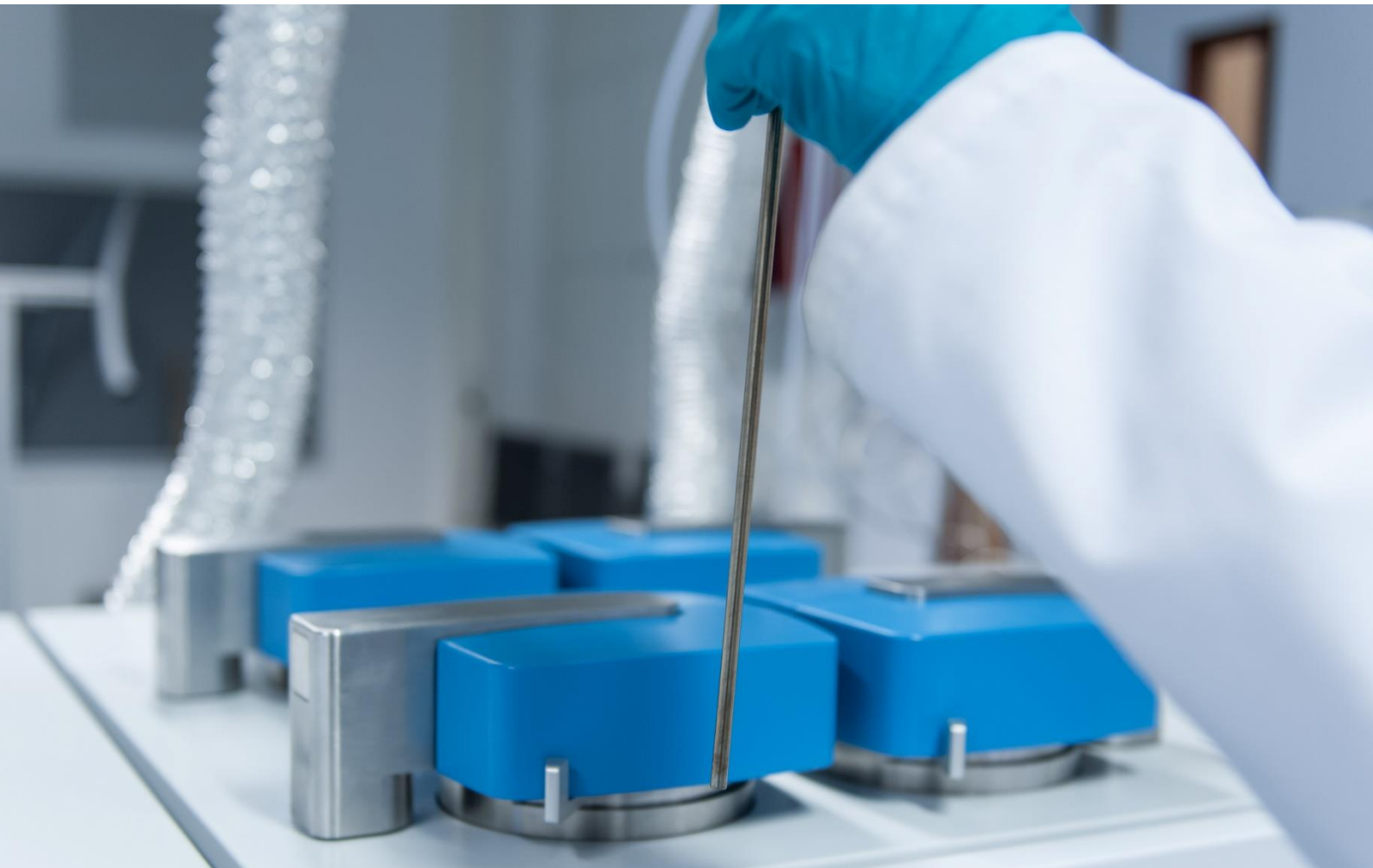

The Flowrence® XR parallel reactor system produces consistent high data quality with outstanding reactor-to-reactor repeatability.

Authors

Tiago Vilela

Graham Ormsby

Robin Jastrzebski

Advantages 4

Introduction 5

Flowrence® XR 6

Experimental Protocol 8

Results 9

Conclusion 13

References 14

Advantages

- Key features of reactor design allow for a reduced influence of exothermic reactions, resulting in more isothermal operation
- Testing of up to 16 separate reactors in parallel
- Downstream dilution with nitrogen results in a rapid quench of the reactor effluent, eliminating sequential homogeneous reactions post catalysis, and control of the effluent concertation for online GC analysis
- The design of the downstream section includes offline liquid sampling for collection of wax products. The wax collection is done in a temperature-controlled sample system that can be varied during the execution of a reaction
- Full headspace analysis of the reactor effluent, with option to include different types of hydrocarbon analysis (e.g. PONA)
- Automatic reconstitution of offline GC data and online data
- Full automated process control with *Flowrence® XR* software

Flowrence® Fischer-Tropsch

Standard Configuration

Customisation on Request

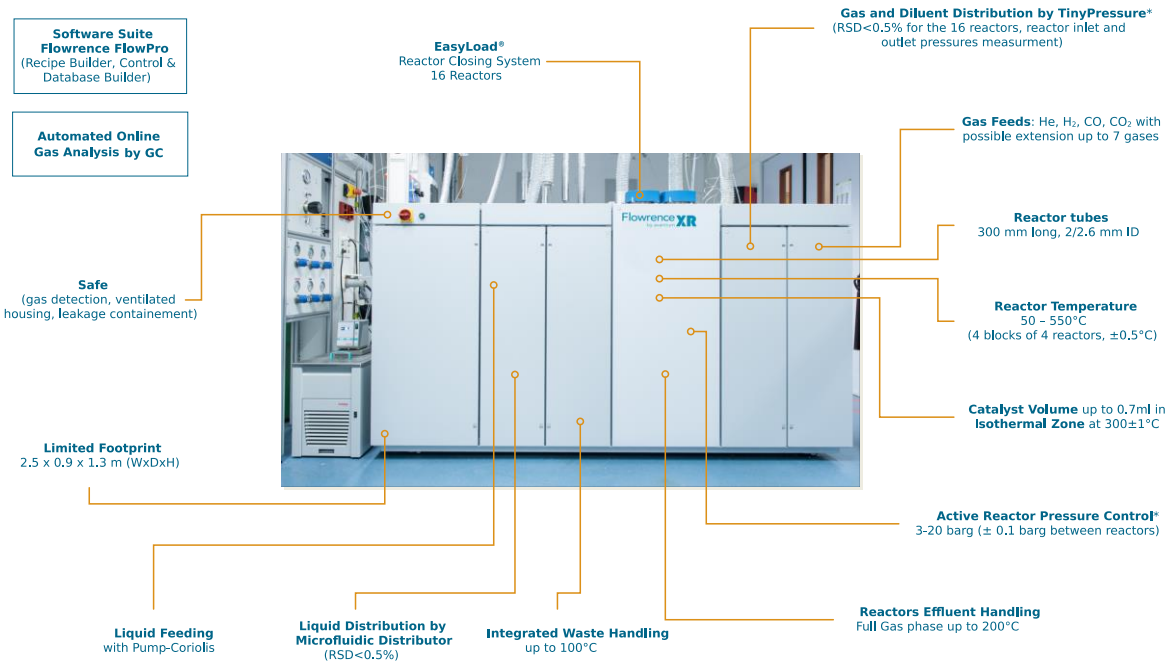

Introduction

Flowrence® high-throughput technology is extensively used for the parallel testing of heterogeneous catalysts over of a wide range of process conditions and applications.

The *Flowrence® XR* testing system can handle the most challenging feedstocks and effluent streams. The 16-parallel reactors with tightly controlled isothermal zones are ideal for Fischer-Tropsch (FT) catalyst research, which requires the handling of wax, water and gas phase products in the effluent stream. In addition, pressure regulation and flow distribution are the most tightly controlled in the industry, ensuring that pressure, flow, space velocity and syngas ratios are constant for all parallel reactors. Avantium has more than 10 units installed worldwide.

To meet the high demand for petrochemicals, FT continues to attract the attention of the researchers and industrial scientists.

The FT process is a challenging reaction to carry out due to its exothermicity, its wide range of products including heavy waxes, catalysts sensitivity to deactivation and the large number of parameters influencing the kinetics. Numerous parameters need to be controlled for accurate data acquisition and correct comparison of catalysts performances. As a consequence, careful control of all process parameters is required to maintain the desired product selectivity.

Generally, FT is operated in the temperature range of 200-300°C. Higher temperatures favor methane formation in detriment of long-chain alkanes. Increasing the pressure leads to higher conversions and higher selectivity to longer chain length but also more heat is produced in the reactor bed which could lead to deactivation. Investigation of FT involves many challenges: a wide variety of products, the need for gas-liquid separation at elevated temperatures, the formation of waxes which affects both gas and liquid flows and the risk of plugging. In addition, there is the need for comparing lifetime tests for syngas feeds varying in composition and poison content.

As the absence of significant temperature gradients is important in kinetic studies, the small-diameter reactor of the Flowrence® makes it also an excellent tool for kinetic studies because the gradient is small. The *Flowrence® XR* is successfully used in academia and industry for a wide range of syngas chemistries including FT [1-28].

In order to verify the quality of the reactor-to-reactor repeatability, Avantium tests each new System for FT applications with a standardized experimental protocol over a range of conversion levels using a reference catalyst synthesized by Avantium.

This article presents the detailed results of such test i.e., Factory Acceptance Test (FAT), quantifying the repeatability of CO conversion, CH_4 selectivity and C5+ selectivity.

Flowrence® XR

Over the past 10 years, Avantium has built several systems for Fischer-Tropsch with 16-parallel reactors. Figure 1 below shows a schematic of a *Flowrence® XR*. The unit employs Flowrence® Technology, which provides tight control of process conditions – temperature, flow rates, and pressure. More information can be found in several patents. [29–33]

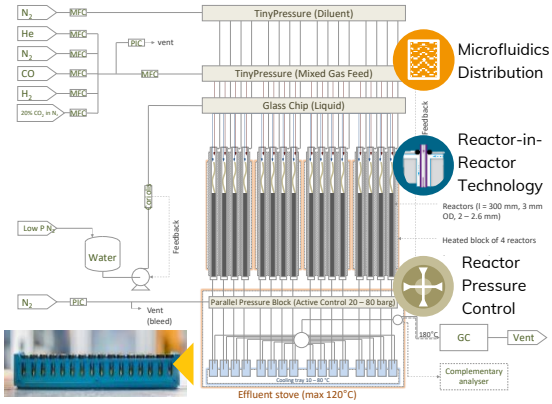

Figure 1: Schematic of Flowrence® XR, configured for FT applications [WO2014062055, WO2014062056, WO2015080572, WO02092219].

Feed Section

The feed section consists of several mass flow controllers (denoted MFC) including reactant gases CO and H_2. *He* is used as an internal standard for online GC quantification. The gas feeds are combined, and measured in a common MFC so that the overall syngas ratio can be kept constant even if the overall GHSV and source flows are changed. The mixed gas feed is then distributed evenly over 16 parallel reactors (flow ±0.5% RSD), using a Microfluidics Distribution Glass Chip (Mixed Gas Feed). The distribution of the diluent is also done using a Microfluidics Distribution Glass Chip (Diluent Gas Feed) and also distributed evenly over 16 parallel reactors (flow ±0.5% RSD). The Tiny Pressure module allows for pressure control and readout of all 16 reactors. Each reactor pressure is regulated via feedback control of real-time pressure and regulated within a bandwidth of ±0.1barg. Water feeding (optional) is provided from an HPLC pump (slave) driven by a Coriolis flowmeter (Master). The water distribution is done through Microfluidics Distribution (±0.5% RSD).

Reaction Section

The reaction section consist of 4 independent temperature controlled blocks with 4 reactors each. The Flowrence system has a patented parallel pressure controller downstream of the reactor (Patent No. WO2006107187, 2006). The reactor pressure controller (denoted PIC) provides the reference pressure. Downstream of the Parallel Pressure Block is at ambient pressure.

A downstream effluent stove houses a sample system. The sample system, robotically controlled, has 4 sample rows, each row consisting of 16 parallel gas/liquid separator vials (8ml).

Both heating and cooling (provided by external chiller) allow for temperature control of the sample system and gas/liquid separators.

The following Table summarizes the standard setup used for the *Flowrence® XR* for FT applications.

Table 1: Summary of a standard Flowrence® XR setup for FT applications.

Reactor setup	16 parallel reactors, arranged in 4*4 blocks, each block independent temperature control (50-550°C)
Reactor details	3mm OD, 2mm ID or 2.6mm ID, reactor length 300/560mm(1), SS316
Gas feed	Passive distribution, of syngas mix using microfluidic distribution (±0.5% RSD reactor-to-reactor relative standard deviation)
Pressure control	All reactors controlled with active pressure control (±0.1 barg) up to 80 barg
Downstream effluent control	4×16 parallel catch pots for wax collection (85°C) and trace heating at 180°C for online analysis of gas phase
Analytics	Online GC, with FID to quantify C1-C12 with other options available upon request (e.g. PONA analysis, alpha determination)

(1) Both options available for Fischer-Tropsch Applications

Product Section

The reactor effluent is separated in the sample vial into a liquid and a gas phase at atmospheric pressure. The sample vials are temperature controlled to optimize the amount of gaseous hydrocarbons that are analyzed by the online GC. The effluent stream is diluted with N_2, to control the GC concentration. The product section gas-liquid separation is optimized using the temperature-controlled sample tray chiller and oven. Of course, these conditions could be optimized for other chemistries, or effluent streams if required.

The headspace analysis is done by *on-line* GC, with a selection valve used to select 1 of 16 samples at any given time, with the non-selected reactor streams going to a common waste line and to vent.

The GC is connected to the *Flowrence® XR* using a heated trace line (temperature-controlled).

On-line analysis (GC): C_1-C_{12} hydrocarbons are analyzed on-line with separation of alkenes/alkanes. Higher alkanes are back flushed. Helium was used as an internal standard to prevent miscalculation due to gas volume change during the reaction.

The complete online GC cycle duration per reactor (analysis + preparation for the next trigger) is estimated to 15min, so a total duration of 4h is required for a full pass on the 16 reactors.

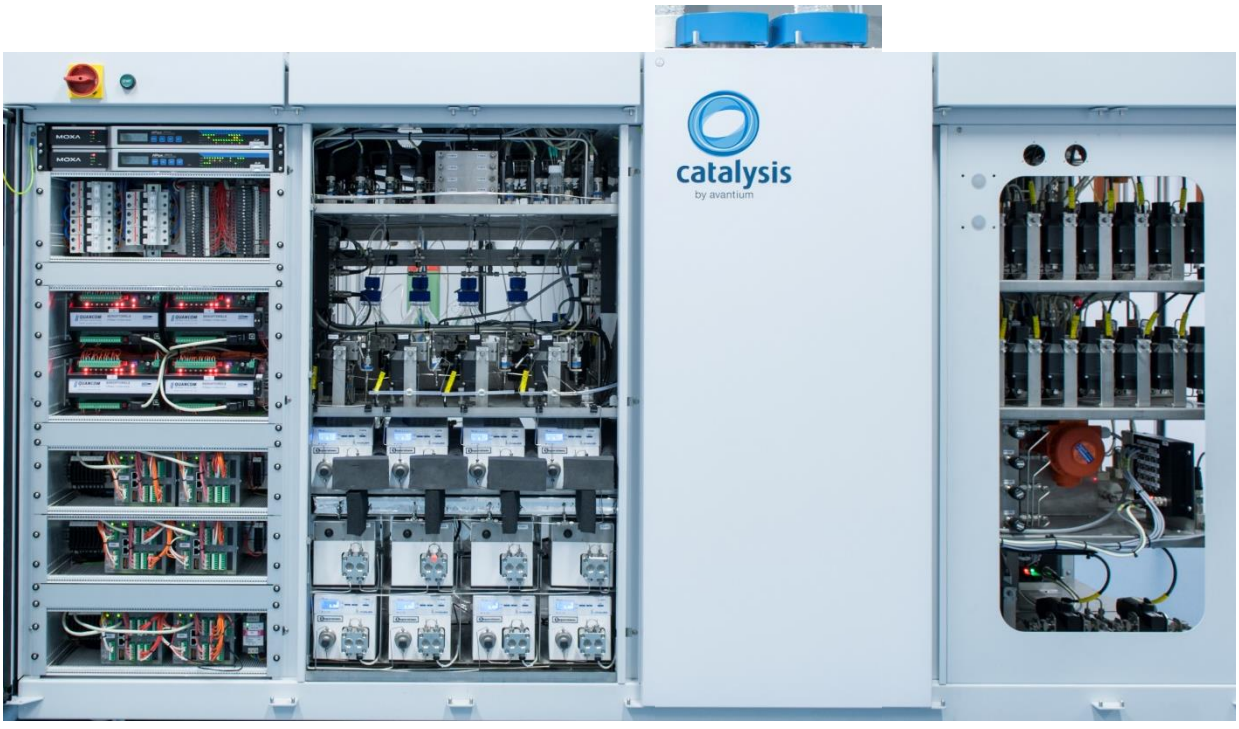

Experimental Protocol

Avantium uses a standardized experimental protocol to validate all Systems for FT application prior to delivery to end user. The protocol is tailored for quickly validating the reactor-to-reactor repeatability. For this we make use of a reference catalyst synthesized by Avantium.

All feed gases were from high-grade supplies. The H_2 (5.0 grade) and CO (4.7 grade) gases were used. A trap a Sulphur Carbonyls removal agents was also used.

The following conditions were fixed for all experiments, whilst the GHSV was varied to get a range of CO conversion levels:

- Reaction pressure 15-25 barg
- CO/H_2 ratio 0.4-0.6 (2-5% He added as GC internal standard)
- GHSV of 10,000h^{-1} and 4,600h^{-1}

The CO conversion was changed by GHSV whilst maintaining the above conditions.

The following protocol was used to activate the catalysts:

1. Catalyst reduction with pure H_2
2. Cooling under pure H_2
3. Catalyst testing and data acquisition

Catalyst and Reactor Loading

The catalyst synthesized by Avantium is being used as a reference material for the chemical validation of our systems for FT studies for more than 10 years. This reference catalyst has a target composition of 0.75 wt.% Re and 25 wt.% Co doped on γ-Al_2O_3.

Each reactor is loaded with an inert diluent material (nonporous ceramic beads 100–200 µm) used as a filler for the catalyst bed. The positioning of the catalyst bed is done so that the catalyst sits in the pre-determined isothermal zone (±1 °C).

Each space velocity condition was achieved by varying the total flow. Catalysts were loaded in a range of 100-225mg.

Results

System Performance

Gas Feed Distribution, Pressure and Temperature
Good control of the process conditions and in particular the distribution of the feed gas is essential for obtaining reliable data. The equal distribution of the gas feed can be monitored by looking at the measured ratio between the internal standard (helium) and the diluent (nitrogen). As neither gas participates in the reaction, the ratio between them should be fixed. Since the two gases are independently distributed over the 16 reactors, the ratio incorporates the error of both the mixed feed gas and diluent distribution. Figure 2 shows the He:N_2 ratio as a function of time on stream.

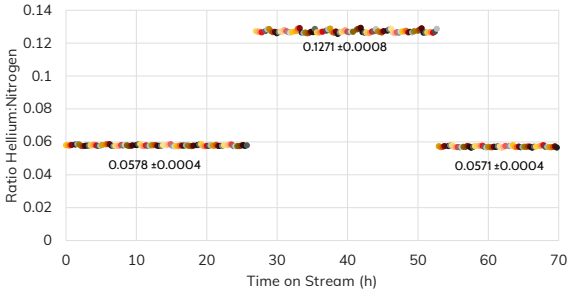

Figure 2: He/N2 ratio as function of time on stream (colors varied by reactor number).

Between 25 to 50 hours time on stream, the system was operated at the high space velocity condition. Since this mixed feed composition was kept constant, but mixed feed flow increased, the amount of helium fed increased concurrently. Within the constant space velocity regimes, the ratio stays constant.

Table 2 presents the mean, standard deviation (SD) and relative standard deviation (RSD) at 2 space velocity conditions tested for all data points for 16 reactors.

The RSD obtained is 0.7% for both GHSV.

Table 2: Reactor-to-reactor deviation of the He:N_2 ratio.

GHSV (h^{-1})	Mean	SD	RSD
4,600	0.0571	0.0004	0.7%
10,000	0.1271	0.0008	0.7%

Figure 3 and Figure 4 show the reactor temperature and pressure as function of time on stream respectively.

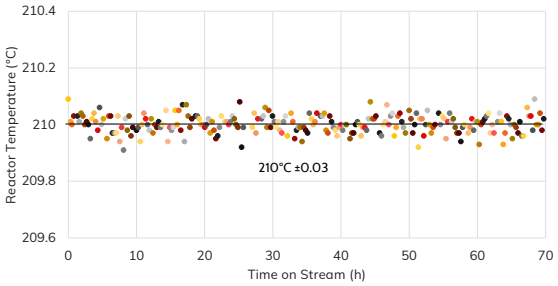

Figure 3: Reactor temperature as function of time on stream (colors varied by reactor number).

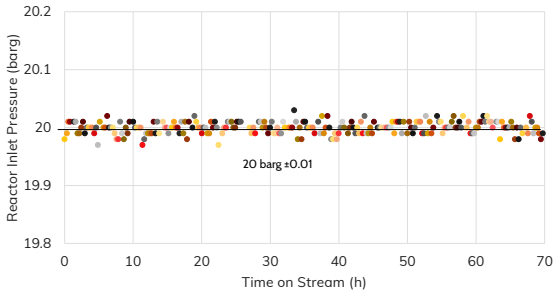

Figure 4: Reactor inlet pressure as a function of time on stream (colors varied by reactor number).

As can be seen, both parameters are tightly controlled during the entire run, with temperature deviations within ±0.03 °C and pressure deviations within ±0.01barg.

Reactor-to-Reactor Reproducibility

The following calculations were used, to calculate the selectivity and conversion.

CO conversion:

$$X_{CO,n} = \frac{(Q_{CO,in,n} - Q_{CO,n})}{Q_{CO,in,n}}$$

Selectivity's:

$$S_{CH_4,n} = \frac{Q_{CH_4,,n}}{(Q_{CO,in,n} - Q_{CO,n})}$$

$$S_{C_{5+},n} = 1 - S_{CH_4,n} - S_{C_2,n} - S_{C_3,n} - S_{C_4,n}$$

Where the symbols represent:

- $Q_{CO,in,n}$ is the volumetric CO inlet flow for reactor n (NmL/min).
- $Q_{CO,n}$ is the volumetric CO outlet flow for reactor n (NmL/min).
- $Q_{CH4,n}$ is the volumetric CH_4 outlet flow for reactor n (NmL/min). The volumetric flow for all products was multiplied by the corresponding carbon number
- $X_{CO,n}$ is the CO conversion for reactor n (dimensionless number).

$S_{X,n}$ is the selectivity to compound X for reactor n (dimensionless number). The outlet flows were determined from online GC analysis and the inlet flows are the inlet gas flows divided by 16 streams.

CO Conversion

Figure 5 shows the reaction profile of the reference test. 15 reactors were loaded with the reference catalyst, and one reactor was loaded with inert material. Two space velocity conditions were performed (4,600, and 10,000 h^{-1}). The blank reactor shows 0% conversion as expected, whilst the other 15 reactors, loaded with replica catalysts show similar trends.

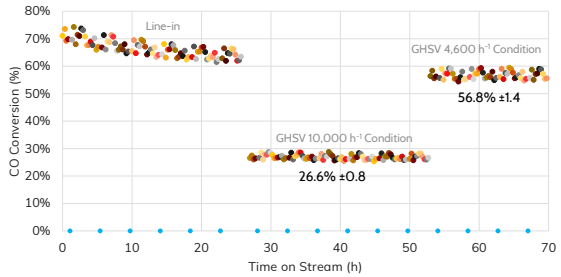

Figure 5: CO conversion as a function of time on stream (colors varied by reactor number).

Figure 5 shows the CO conversion as a function of time on stream and clearly shows the different phases of the experiment: the line-in occurs in in first 25h at ~4,600 h^{-1}. The following 25h period is the high space velocity (~10,000 h^{-1}) regime and low conversion, with relatively low conversion. The final 20h period is the low space velocity
(~4,600 h^{-1}) regime and clearly shows still on-going catalyst line-in.

The reactor-to-reactor repeatability for the CO conversion is shown in Figure 6 and Figure 7.

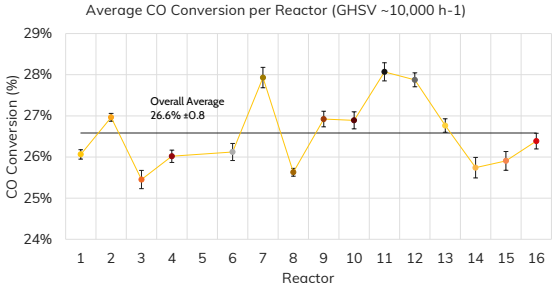

Figure 6: Average CO conversion and SD per reactor for GHSV ~ 10,000 h^{-1}. Reactor 5 (blank) has been omitted for clarity.

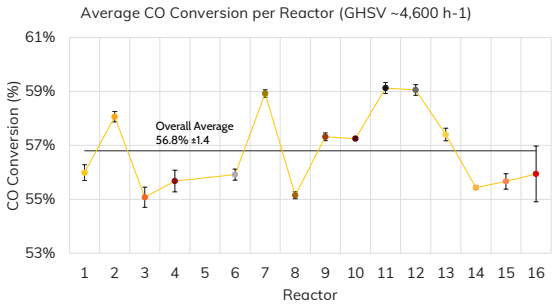

Figure 7: Average CO conversion and SD per reactor for GHSV ~4,600 h^{-1}. Reactor 5 (blank) has been omitted for clarity.

These plots are useful for comparing the reactor-to-reactor variability and we can see that a small activity differences exist between reactors, which are consistent among them. As CO conversion is non-linearly dependent on temperature and space velocity, small differences in both may still lead to measurable differences in activity.

The mean, standard deviation and relative standard deviation for reactor-to-reactor deviations are shown in Table 3. Again, although deactivation is overlaid in this data, this is (mostly) averaged out by averaging over the entire time on stream data set. The observed standard deviations are 0.8% and 1.4%.

Table 3: Reactor-to-reactor deviation of CO conversion.

GHSV h^{-1}	Mean	SD	RSD
10,000	26.6%	0.8%	3.16%
4,600	56.8%	1.4%	2.54%

CH_4 and C_{5+} Selectivity

The selecitivity towards methane as a function of time on stream is shown in Figure 8. Again, the two space velocity regimes can be clearly distinguished.

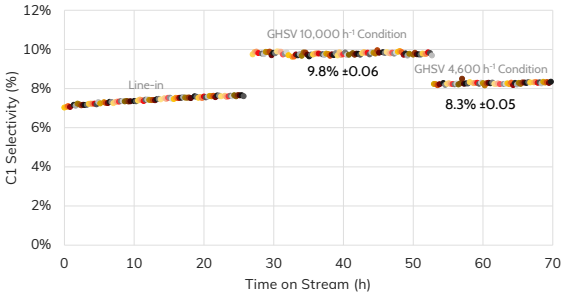

Figure 8: Methane selectivity as a function of time on stream (colors varied by reactor number).

At first glance, the selectivity in the high space velocity regime seems noisier than in the low space velocity regime, but this is to be expected as a similar absolute error is divided by much smaller fraction of converted CO. Further examination of the spread of the data in Figure 8 shows that most spread is actually attributable to measurement error which is averaged out over multiple data points. This is reflected in the standard deviation in reactor-to-reactor reapeatability of 0.1% SD (Table 4).

Table 4: Reactor-to-reactor deviation of C1 and C5+ selectivity.

Attribute	GHSV h^{-1}	Mean	SD	RSD
C1 Selectivity	10,000	9.8%	0.1%	0.7%
C1 Selectivity	4,600	8.3%	0.1%	0.6%
C5+ Selectivity	10,000	81.0%	0.1%	0.2%
C5+ Selectivity	4,600	83.4%	0.1%	0.2%

The C5+ selectivity (Table 4 and Figure 9) shows similar trends with a standard deviation in reactor-to-reactor reapeatability of also 0.1% SD.

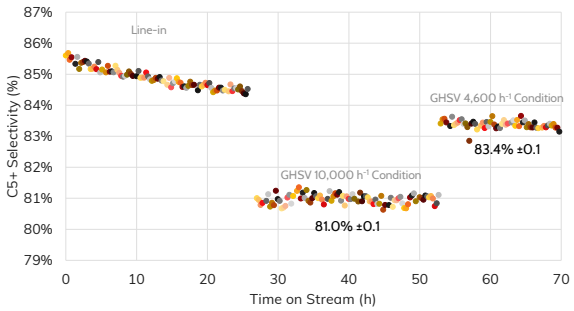

Figure 9: C5+ selectivity as a function of time on stream (colors varied by reactor number).

Figure 10 and Figure 11 show the outstanding reactor-to-reactor variability for both space velocity conditions.

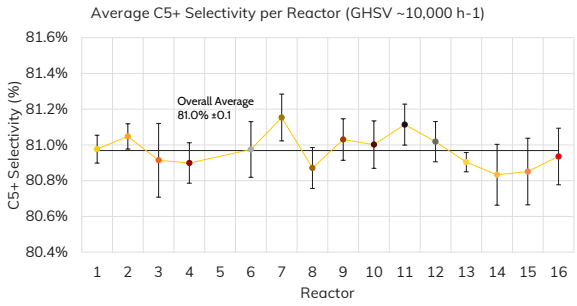

Figure 10: Average C5+ selectivity and SD per reactor for condition GHSV ~ 10,000 h-1. Reactor 5 (blank) has been omitted for clarity.

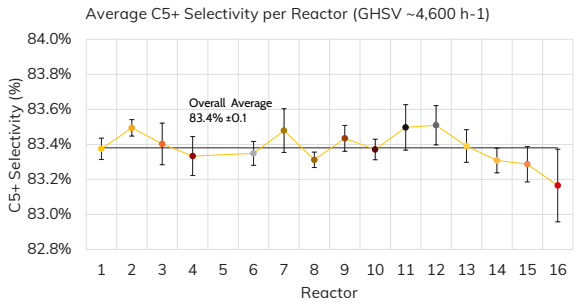

Figure 11: Average C5+ selectivity and SD per reactor for condition GHSV ~4,600 h-1. Reactor 5 (blank) has been omitted for clarity.

Alpha number

The chain growth probability alpha (α) according to the Anderson-Flory-Schulz distribution is an important parameter for Fischer-Tropsch catalyst performance. Although frequently determined by measuring the product distribution of collected wax products using SimDist, the online GC of the Flowrence allows on-line determination of α, based on the fraction of low boiling substances. The ASF distribution is linearized by plotting the natural log of the mole fraction as function of the carbon number. The slope of the line corresponds to natural logarithm of α. The plot of a typical distribution in the described experiment is shown in Figure 12.

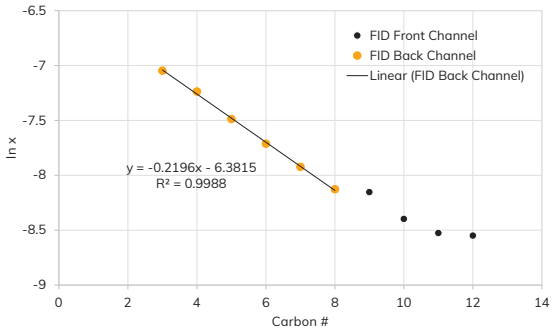

Figure 12: Alpha determination for a single data point using C3–C8.

As the analyzed sample is split over the FID front and back channels on the GC to speed up analysis, a small discontinuity can be observed when switching channels; the most reliable fit is therefore obtained by fitting only the components measured on the FID front channel (C3–C8). The α is then calculated for every collected data point and a good fit ($R^2 > 0.998$) is then obtained. Since every reactor is measured every 15 min, it is possible to make a linearization of the data per every injection (i.e. α can be made function of time-on-stream). A plot of the determined α as a function of time on stream, as well as the corresponding R^2 are shown in Figure 13.

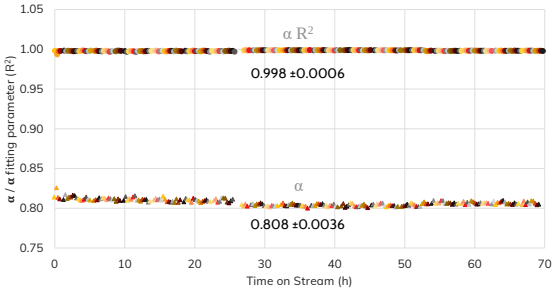

Figure 13: Alpha as a function of time on stream (colors varied by reactor number).

The α has only a very weak dependence on the reaction condition; the mean α is 0.808, with a relatively high average 0.811 during the initial 25h line-in period. In addition, α R^2 stays high during the entire run, showing a consistent good fitting of α.

Conclusion

The ***Flowrence®*** ***XR*** parallel reactor system produces consistent high data quality with outstanding reactor-to-reactor repeatability.
In addition, the system was shown to perform well mechanically and the **α** chain growth probability factor could be consistently obtained by on-line GC data.

The conversion and selectivity of the reactor measured by online GC show an outstanding reactor-to-reactor repeatability:

- Outstanding control of the operating conditions, with relative standard deviations of 0.01% RSD for Temperature, 0.05% RSD for Pressure, and 0.7% RSD for the feed distribution over the 16 reactors at both GHSV conditions
- The reactor-to-reactor repeatability for *CO Conversion* was 1.4% SD and 0.8% SD for GHSV 4,600 and 10,000, respectively
- The reactor-to-reactor repeatability for *C1 Selectivity* was 0.1% SD for both GHSV conditions
- The reactor-to-reactor repeatability for *C5+ Selectivity* was also 0.1% SD for both GHSV conditions

References

[1] Wang, J.; Huang, S.; Howard, S.; Muir, B. W.; Wang, H.; Kennedy, D. F.; Ma, X. Elucidating Surface and Bulk Phase Transformation in Fische-Tropsch Synthesis Catalysts and Their Influences on Catalytic Performance. ACS Catal. 2019, 9 (9), 7976-7983.

[2] van Deelen, T. W.; Nijhuis, J. J.; Krans, N. A.; Zečević, J.; de Jong, K. P. Preparation of Cobalt Nanocrystals Supported on Metal Oxides To Study Particle Growth in Fischer–Tropsch Catalysts. ACS Catal. 2018, 8 (11), 10581–10589.

[3] Chen, Y.; Batalha, N.; Marinova, M.; Impéror-Clerc, M.; Ma, C.; Ersen, O.; Baaziz, W.; Stewart, J. A.; Curulla-Ferré, D.; Khodakov, A. Y.; et al. Ruthenium Silica Nanoreactors with Varied Metal–Wall Distance for Efficient Control of Hydrocarbon Distribution in Fischer–Tropsch Synthesis. Journal of Catalysis 2018, 365, 429–439.

[4] Carvalho, A.; Marinova, M.; Batalha, N.; Marcilio, N. R.; Khodakov, A. Y.; Ordomsky, V. V. Design of Nanocomposites with Cobalt Encapsulated in the Zeolite Micropores for Selective Synthesis of Isoparaffins in Fischer–Tropsch Reaction. Catal. Sci. Technol. 2017, 7 (21), 5019–5027.

[5] Oschatz, M.; Hofmann, J. P.; van Deelen, T. W.; Lamme, W. S.; Krans, N. A.; Hensen, E. J. M.; de Jong, K. P. Effects of the Functionalization of the Ordered Mesoporous Carbon Support Surface on Iron Catalysts for the Fischer–Tropsch Synthesis of Lower Olefins. ChemCatChem 2017, 9 (4), 620–628.

[6] Ordomsky, V. V.; Khodakov, A. Y. Syngas to Chemicals: The Incorporation of Aldehydes into Fischer–Tropsch Synthesis. ChemCatChem 2017, 9 (6), 1040–1046.

[7] Mejía, C. H.; Otter, J. H. den; Weber, J. L.; Jong, K. P. de. Crystalline Niobia with Tailored Porosity as Support for Cobalt Catalysts for the Fischer–Tropsch Synthesis. Applied Catalysis A: General 2017, 548, 143–149.

[8] Botes, G. F.; Bromfield, T. C.; Coetzer, R. L. J.; Crous, R.; Gibson, P.; Ferreira, A. C. Development of a Chemical Selective Iron Fischer Tropsch Catalyst. Catalysis Today 2016, 275

[9] Subramanian, V.; Ordomsky, V. V.; Legras, B.; Cheng, K.; Cordier, C.; Chernavskii, P. A.; Khodakov, A. Y. Design of Iron Catalysts Supported on Carbon–Silica Composites with Enhanced Catalytic Performance in High-Temperature Fischer–Tropsch Synthesis. Catal. Sci. Technol. 2016, 6 (13), 4953–4961.

[10] Delgado, J. A.; Claver, C.; Castillón, S.; Curulla-Ferré, D.; Ordomsky, V. V.; Godard, C. Effect of Polymeric Stabilizers on Fischer–Tropsch Synthesis Catalyzed by Cobalt Nanoparticles Supported on TiO2. Journal of Molecular Catalysis A: Chemical 2016, 417, 43–52.

[11] Cheng, K.; Subramanian, V.; Carvalho, A.; Ordomsky, V. V.; Wang, Y.; Khodakov, A. Y. The Role of Carbon Pre-Coating for the Synthesis of Highly Efficient Cobalt Catalysts for Fischer–Tropsch Synthesis. Journal of Catalysis 2016, 337, 260–271.

[12] Subramanian, V.; Cheng, K.; Lancelot, C.; Heyte, S.; Paul, S.; Moldovan, S.; Ersen, O.; Marinova, M.; Ordomsky, V. V.; Khodakov, A. Y. Nanoreactors: An Efficient Tool To Control the Chain-Length Distribution in Fischer–Tropsch Synthesis. ACS Catal. 2016, 6 (3), 1785–1792.

[13] den Otter, J. H.; Nijveld, S. R.; de Jong, K. P. Synergistic Promotion of Co/SiO2 Fischer–Tropsch Catalysts by Niobia and Platinum. ACS Catal. 2016, 6 (3), 1616–1623.

[14] den Otter, J. H. den; Yoshida, H.; Ledesma, C.; Chen, D.; Jong, K. P. de. On the Superior Activity and Selectivity of PtCo/Nb2O5 Fischer Tropsch Catalysts. Journal of Catalysis 2016, 340, 270–275.

[15] Oschatz, M.; Lamme, W. S.; Xie, J.; Dugulan, A. I.; Jong, K. P. de. Ordered Mesoporous Materials as Supports for Stable Iron Catalysts in the Fischer–Tropsch Synthesis of Lower Olefins. ChemCatChem 2016, 8 (17).

[16] Oschatz, M.; Krans, N.; Xie, J.; Jong, K. P. de. Systematic Variation of the Sodium/Sulfur Promoter Content on Carbon-Supported Iron Catalysts for the Fischer–Tropsch to Olefins Reaction. Journal of Energy Chemistry 2016, 25 (6), 985–993.

[17] Ordomsky, V. V.; Carvalho, A.; Legras, B.; Paul, S.; Virginie, M.; Sushkevich, V. L.; Khodakov, A. Y. Effects of Co-Feeding with Nitrogen-Containing Compounds on the Performance of Supported Cobalt and Iron Catalysts in Fischer–Tropsch Synthesis. Catalysis Today 2016, 275, 84–93.

[18] Eschemann, T. O.; Oenema, J.; Jong, K. P. de. Effects of Noble Metal Promotion for Co/TiO2 Fischer-Tropsch Catalysts. Catalysis Today 2016, 261, 60–66.

[19] Cheng, K.; Ordomsky, V. V.; Legras, B.; Virginie, M.; Paul, S.; Wang, Y.; Khodakov, A. Y. Sodium-Promoted Iron Catalysts Prepared on Different Supports for High Temperature Fischer–Tropsch Synthesis. Applied Catalysis A: General 2015, 502, 204–214.

[20] Eschemann, T. O.; Lamme, W. S.; Manchester, R. L.; Parmentier, T. E.; Cognigni, A.; Rønning, M.; de Jong, K. P. Effect of Support Surface Treatment on the Synthesis, Structure, and Performance of Co/CNT Fischer–Tropsch Catalysts. Journal of Catalysis 2015, 328, 130–138

[21] Eschemann, T. O.; de Jong, K. P. Deactivation Behavior of Co/TiO2 Catalysts during Fischer–Tropsch Synthesis. ACS Catal. 2015, 5 (6), 3181–3188.

[22] Cheng, K.; Virginie, M.; Ordomsky, V. V.; Cordier, C.; Chernavskii, P. A.; Ivantsov, M. I.; Paul, S.; Wang, Y.; Khodakov, A. Y. Pore Size Effects in High-Temperature Fischer–Tropsch Synthesis over Supported Iron Catalysts. Journal of Catalysis 2015, 328, 139–150.

[23] Munnik, P.; Krans, N. A.; de Jongh, P. E.; de Jong, K. P. Effects of Drying Conditions on the Synthesis of Co/SiO2 and Co/Al2O3 Fischer–Tropsch Catalysts. ACS Catal. 2014, 4 (9), 3219–3226.

[24] Eschemann, T. O.; Bitter, J. H.; de Jong, K. P. Effects of Loading and Synthesis Method of Titania-Supported Cobalt Catalysts for Fischer–Tropsch Synthesis. Catalysis Today 2014, 228, 89–95.

[25] Munnik, P.; de Jongh, P. E.; de Jong, K. P. Control and Impact of the Nanoscale Distribution of Supported Cobalt Particles Used in Fischer–Tropsch Catalysis. J. Am. Chem. Soc. 2014, 136 (20), 7333–7340.

[26] en Otter, J. H.; de Jong, K. P. Highly Selective and Active Niobia-Supported Cobalt Catalysts for Fischer–Tropsch Synthesis. Top Catal 2014, 57 (6), 445–450.

[27] riboval-Constant, A.; Butel, A.; Ordomsky, V. V.; Chernavskii, P. A.; Khodakov, A. Y. Cobalt and Iron Species in Alumina Supported Bimetallic Catalysts for Fischer–Tropsch Reaction. Applied Catalysis A: General 2014, 481, 116–126.

[28] Cheng, K.; Ordomsky, V. V.; Virginie, M.; Legras, B.; Chernavskii, P. A.; Kazak, V. O.; Cordier, C.; Paul, S.; Wang, Y.; Khodakov, A. Y. Support Effects in High Temperature Fischer-Tropsch Synthesis on Iron Catalysts. Applied Catalysis A: General 2014, 488, 66–77.

[29] de Ruiter, R. R.; Bracht, M.; Gruter, G. J. M. EP 2263790 A3, 2011.

[30] Moonen, R. H. W. WO2012047095A1, 2012.

[31] Moonen, R. H. W. U.S. Patent 20,160,121,291 A1, 2016.

[32] Smit, M.; Gruter, G. J. M. U.S. Patent 7,997,297 B2, 2011.

[33] Van den Brink, P. J.; Bracht, M.; Harji, B. H. WO2002092219A1, 2002.